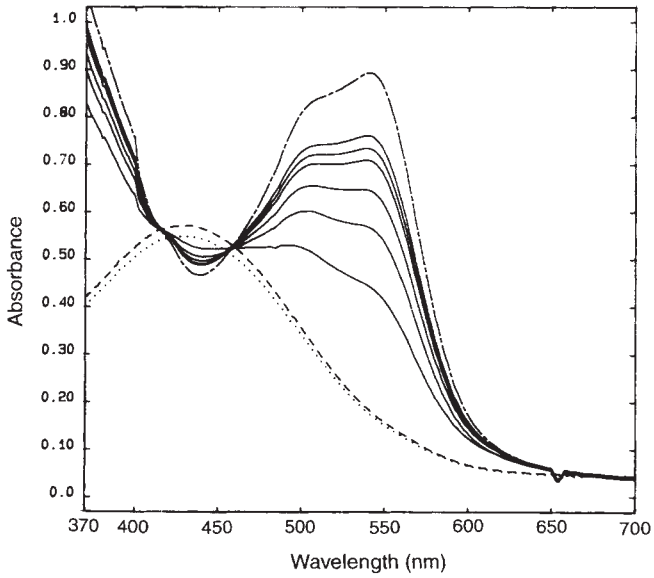

FIG. 3 Ultraviolet–visible absorption spectra of **5**-Fe(III) (dashed line) and **5**-Fe(II) (dot-dashed line), (0.25 mM concentration in MeOH : aqueous Tris buffer (9 : 1 ratio), pH 7.5); also shown are changes of the spectrum of **5**-Fe(III) (solid lines) on treatment with ascorbic acid (fivefold excess, 15-s intervals), and the spectrum (dotted line) after treatment with ammonium persulphate (tenfold excess).

but become increasingly aligned in a chiral sense when the internal **5**-Fe(III) complex is converted to the external **5**-Fe(II) complex and the dinuclear **5**-Fe(III)/Fe(II) complex. (This dinuclear complex was prepared by treatment of **5** with one equivalent of $FeSO_4$ and one equivalent of $FeCl_3$. The absorption spectrum of the dinuclear complex in the visible region is a superposition of those obtained from the corresponding mononuclear complexes **5**-Fe(II) and **5**-Fe(III), and lacks new charge-transfer bands. This excludes the occurrence of metal–metal interactions.) This is shown by the circular dichroism spectra of these complexes which reveal increasing Cotton effects in the 290-nm region due to exciton coupling between the bipyridyl groups (Table 1)[36]. It may accordingly be concluded that the internal metal centre directs and amplifies the chirality of the external one. Moreover, the reductive switching process seems to occur diastereoselectively, as the alignment of the bipyridyl chromophores intensifies during the reduction of **5**-Fe(III) to **5**-Fe(II). On re-oxidation, the internal **5**-Fe(III) complex is regenerated, although equilibration to its original left-handed configuration is only established after several hours. The rather slow regeneration of the left-handed **5**-Fe(III) complex is probably due to the rather drastic oxidation conditions; but the possibility that the oxidized Fe(III) is solvated before its recapture by the hydroxamate ligand cannot be excluded.

The molecular switches introduced here are intended to contribute to the future development of molecule-based technologies, although significant improvements in their performance are still needed. The challenges that remain to be addressed include developing a means to stimulate switching by electrochemical and photochemical means, improving their addressing, reading and response rate, and finding ways of immobilizing them on conducting surfaces. □

Received 16 December 1994; accepted 22 March 1995.

1. Carter, F. L. *Molecular Electronic Devices II* (Dekker, New York, 1987).
2. Hopfield, J. J., Onuchic, J. N. & Beratan, D. N. *J. phys. Chem.* **93,** 6350–6357 (1989).
3. Lehn, J. M. *Angew. Chem. int. Edn engl.* **29,** 1304–1319 (1990).
4. Wild, U. P., Bernet, S., Kohler, B. & Renn, A. *Pure appl. Chem.* **64,** 1335–1342 (1992).
5. Anders, J. *et al. Ber. Bunsenges. phys. Chem.* **97,** 483–487 (1993).
6. Rubinstein, I., Steinberg, S., Tor, Y., Shanzer, A. & Sagiv, J. *Nature* **332,** 426–429 (1988).
7. Huston, M. E., Akkaya, E. U. & Czarnik, A. W. *J. Am. chem. Soc.* **111,** 8735–8737 (1989).
8. Bissell, R. A. *et al. Chem. Soc. Rev.* **21,** 187–195 (1992).
9. Aviram, A. & Ratner, M. A. *Chem. Phys. Lett.* **29,** 277–283 (1974).
10. Pomerantz, M., Aviram, A., McCorkle, A., Li, L. & Schrott, A. G. *Science* **255,** 1115–1118 (1992).
11. Martin, A. S., Sambles, J. R. & Ashwell, G. J. *Phys. Rev. Lett.* **70,** 218–221 (1993).
12. de Silva, A. P., Gunaratne, H. Q. N. & McCoy, C. P. *Nature* **364,** 42–44 (1993).
13. Feringa, B. L., Jager, W. F. & de Lange, B. *J. Am. chem. Soc.* **113,** 5468–5470 (1991).
14. Wasielewski, M. R., O'Neil, M. P., Gosztola, D., Niemczyk, M. P. & Svec, W. A. *Pure appl. Chem.* **64,** 1319–1325 (1992).
15. Gilat, S. L., Kawai, S. H. & Lehn, J. M. *J. chem. Soc., chem. Commun.* 1439–1442 (1993).
16. Goulle, V., Harriman, A. & Lehn, J. M. *J. chem. Soc., chem. Commun.* 1034–1036 (1993).
17. Voegtle, F., Mueller, W. M., Mueller, U., Bauer, M. & Rissanen, K. *Angew. Chem. int. Edn engl.* **32,** 1295–1297 (1993).
18. Bissell, R. A., Cordova, E., Kaifer, A. G. & Stoddart, J. F. *Nature* **369,** 133–137 (1994).
19. Joulie, L. F., Schatz, E., Ward, M. D., Weber, F. & Yellowlees, L. J. *J. chem. Soc., Dalton Trans.* 799–804 (1994).
20. Aviram, A. *Int. J. Quantum Chem.* **42,** 1615–1624 (1992).
21. Livoreil, A., Dietrich-Buchecker, C. O. & Sauvage, J.-P. *J. Am. chem. Soc.* **116,** 9399–9400 (1994).
22. Tor, Y. *Artificial Tripodal Ligands: Design, Synthesis and Properties* (Weizmann Inst. of Science, Rehovot, Israel, 1990).
23. Libman, J., Tor, Y. & Shanzer, A. *J. Am. chem. Soc.* **109,** 5880–5881 (1987).
24. Kraemer, R., Lehn, J.-M., Cian, A. D. & Fischer, J. *Angew. Chem. int. Edn. engl.* **32,** 703–705 (1993).
25. Lehn, J.-M. *et al. Proc. natn. Acad. Sci. U.S.A.* **84,** 2565–2569 (1987).
26. Williams, A. F., Piguet, C. & Bernadinelli, G. *Angew. Chem. int. Edn engl.* **30,** 1490–1492 (1991).
27. Piguet, C., Hopfgartner, G., Bocquet, B., Schaad, O. & Williams, A. F. *J. Am. chem. Soc.* **116,** 9092–9102 (1994).
28. Constable, E. C. *Angew. Chem. int. Edn. engl.* **30,** 1450–1451 (1991).
29. Constable, E. C., Hannon, M. J. & Tocher, D. A. *Angew. Chem. int. Edn engl.* **31,** 230–232 (1992).
30. Raymond, K. N., Mueller, G. & Matzanke, B. F. *Top Curr. Chem.* **123,** 49–102 (1984).
31. Hawker, P. N. & Twigg, M. V. (eds Wilkinson, G., Gillard, R. D. & McCleverty, J. A.) 1179–1288 (Pergamon, Oxford, 1987).
32. Gafni, Y., Weizman, H., Libman, J., Shanzer, A. & Rubinstein, I. *J. Am. chem. Soc.* (submitted).
33. van der Helm, D., Baker, J. R., Eng-Wilmot, D. L., Hossain, M. B. & Loghry, R. A. *J. Am. chem. Soc.* **102,** 4224–4231 (1980).
34. Emery, T. & Neilands, J. B. *J. Am. chem. Soc.* **82,** 3659–3662 (1960).
35. Burgess, J. & Prince, R. H. *J. chem. Soc., A* 1772–1775 (1966).
36. Saito, Y. in *Topics in Stereochemistry* Vol. 10 (eds Eliel, F. L. & Allinger, N. L.) 95–174 (Wiley, New York, 1978).

ACKNOWLEDGEMENTS. This work was supported by the Israel Science Foundation and the Consortium of German Chemical Companies. A.S. is the Siegfried and Irma Ullmann Professor at the Weizman Institute of Science.

Spontaneous assembly of a hinged coordination network

Geoffrey B. Gardner*, D. Venkataraman†, Jeffrey S. Moore†‡ & Stephen Lee*‡

* Department of Chemistry, University of Michigan, Ann Arbor, Michigan 48109, USA
† Departments of Chemistry, and Materials Science and Engineering, University of Illinois, Urbana, Illinois 61801, USA

THE field of supramolecular chemistry has advanced to a stage at which it is possible to select building blocks that will self-assemble into structures with specific network topologies[1–3]. This makes possible the rational design and synthesis of molecular solids with potentially interesting properties. Here we report the construction of open, hinged networks from molecular building blocks. This class of materials has been predicted to exhibit unusual mechanical properties, including auxetic behaviour (negative Poisson's ratio) and negative coefficients of thermal expansion[4–6]. Our approach relies on the notion that rigid organic molecules of high symmetry will adopt one of only a few possible structures when linked via hydrogen bonds or coordination to metals[7–9]. We use trigonal ligands to make networks joined at the vertices by metal ions; the resulting networks are homeotypic[10] with the honeycomb-like AlB_2 and the hinge-like $ThSi_2$ phases. The hinge-like network has channels of inner diameter 15 Å, within which included molecules can be exchanged while the framework remains intact. We have not yet determined whether this material is auxetic.

‡ To whom correspondence should be addressed.

Structures based on three-connected nets such as AlB_2 and $ThSi_2$ have evoked wide attention[4,11–13]. Particular networks in this family are predicted to have unusual mechanical, thermal and electrical properties, especially when they contain large open features. Although syntheses of fragments of these prototypes have been achieved, extensions to three-dimensional networks by conventional synthesis have been difficult to realize[11,14]. One approach to the rational design of crystalline solids has been to use organic molecules which, by their coordinating propensities, their geometry and their relative stoichiometries, are naturally predisposed to form one of several well categorized solid structure types. Structures recently prepared by this method include molecular analogues of the diamond, rutile, simple cubic and the PtS structures[9,15,16]

Following this building-block approach[17–19], we can imagine constructing the AlB_2 or $ThSi_2$ structures by replacing the parent atoms in these lattices with ligands and metal ions whose bonding propensities favour local trigonal geometry. The exact analogues for such a replacement are the LaPtSi (a $ThSi_2$ derivative)[20] and the CaCuP (an AlB_2 derivative)[21] structure types. The 'noble' metal (Pt or Cu) atoms would be replaced by a three-coordinate metal atom, and the main-group (Si or P) atoms by the three-fold symmetric tritopic ligand. The electropositive La or Ca atom positions would be replaced by a non-coordinating anionic counter-ion. Trigonal geometries for the tritopic ligands could be realized in the 1,3,5-functionalized benzene units. We chose Ag(I) as the metal ion, as it is known to exhibit three-fold coordination. The counter-ions were chosen to be the weakly coordinating triflate (trifluoromethanesulphonate, $CF_3SO_3^-$).

The simplest tritopic molecule to consider is 1,3,5-triazine. However, molecular models based on the LaPtSi and CaCuP lattices using triazine building blocks and typical Ag···N distances of 2.2 Å indicate that these hypothetical networks are too crowded. Hence higher homologues were chosen as ligands. The trigonal ligands 1,3,5-tricyanobenzene (TCB) (**1**) and 1,3,5-tris(4-ethynylbenzonitrile)benzene (TEB) (**2**) were synthesized according to well established procedures[22,23]. Nitriles were chosen as the ligating groups as they readily coordinate to the soft Ag(I) cation in a low-coordinate fashion. Crystals of $[Ag(TCB)(CF_3SO_3)]$ and $[Ag(TEB)CF_3SO_3]$ suitable for X-ray analysis were obtained by mixing the constituent molecules in benzene and cooling from elevated temperatures.

TABLE 1 Crystal data for compound **3** and **4** at 27 °C

	TCB·AgOTf (**3**)	TEB·AgOTf (**4**)
Crystal system	Trigonal	Orthorhombic
Space group	$P3_2$ (145)	*Pnn*2 (34)
Cell parameters	$a=b=10.582$ (2) Å $c=10.665$ (3) Å $\alpha=\beta=90°$ $\gamma=120°$	$a=11.592$ (1) Å $b=19.099$ (2) Å $c=38.749$ (4) Å $\alpha=\beta=\gamma=90°$
Z	3	4
Volume	1034.2 (3) Å^3	8584.1 (15) Å^3
No. of reflections refined	2,726	6,448
No. of parameters	208	313
Unweighted agreement factor (R_1)	0.036 ($F>4\sigma$) 0.043 (all data)	0.137 ($F>4\sigma$) (isotropic) 0.235 (all data) 0.1063 (for 2,490 > 4σ reflections for $2\theta<35°$
Weighted agreement factor (weighted R_2)	0.0798 (all data)	0.2867 (all data)
	0.0770 ($F_0>4\sigma$)	0.2644 ($F_0>4\sigma$)*
Highest peak in final difference map	0.26 e Å^{-3}	0.54 e Å^{-3}
Goodness of fit	1.04	1.64

Experimental details for **3**: diffractometer, Syntex $P2_1$ IV; λ(Mo Kα) = 0.710734 Å, Lp corrected; 8,153 reflections collected; computing structure solution, SHELXTL PLUS; computing structure refinement, SHELXL-93[29]; reflections were refined based on F_0^2 by full matrix least squares. Experimental details for **4**: diffractometer, Siemens SMART system with a CCD (charge-coupled device) detector; λ(Mo Kα) = 0.710734 Å, Lp corrected; 6,448 reflections collected; structure solution and refinement, as for **4**. For original data, see Supplementary Information.

* Suitable weights were chosen to obtain smaller estimated standard deviations (e.s.d.s) rather than the recommended weights by SHELXL-93.

The crystal structure of $[Ag(TCB)(CF_3SO_3)]$ (**3**) is shown in Fig. 1*A*. It is homeotypic with the CaCuP structure type (Fig. 1*B*). The crystal structure is trigonal and consists of honeycomb sheets based on alternating 1,3,5-tricyanobenzene and Ag(I) units. Within each sheet, the silver ions are trigonally coordinated to three nitriles in an end-on arrangement at a distance

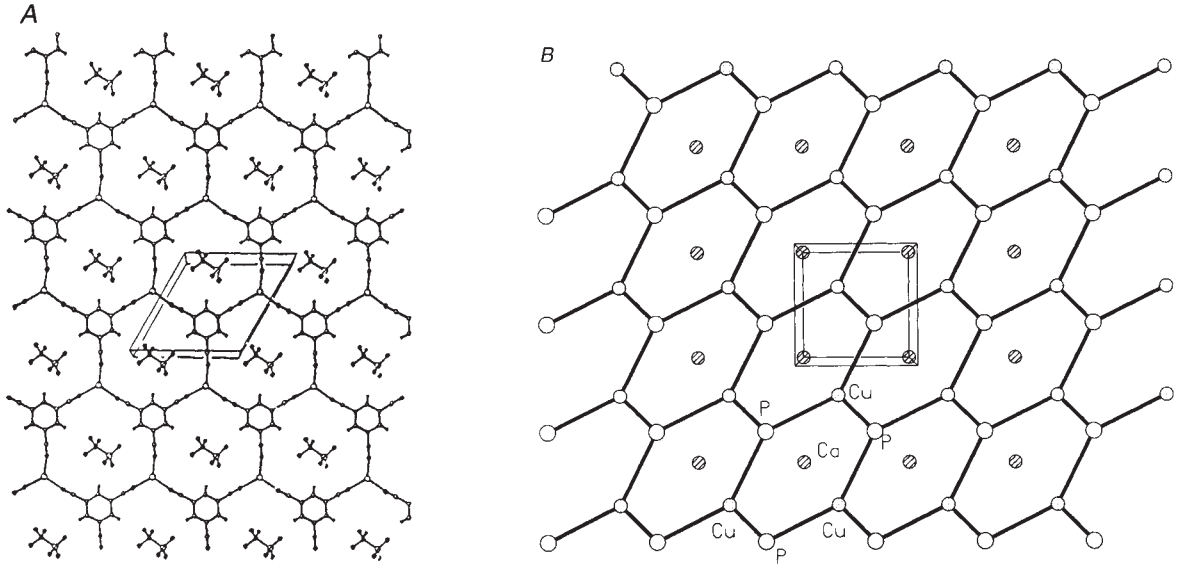

FIG. 1 *A*, Single-layer motif from the crystal structure of **3** parallel to the (001) plane. The triflate coordinates to the Ag(I) ion in the adjacent layer. *B*, Single-layer motif of prototype CaCuP.

of 2.261 Å (N–Ag–N angle, 114.9°; N–Ag–N angle, 122.0°). The layers are separated by 3.55 Å and repeat in an ··ABCABC·· stacking sequence. The honeycomb sheets create cavities of diameter 10.03 Å. The triflate ions are weakly coordinated to the silver in the layer at the axial position of a trigonal pyramid at a distance of 2.390 Å, and consequently occupy the cavity space in an adjacent layer The $[Ag(TCB)(CF_3SO_3)]$ crystal therefore does not have an open channel structure. The final crystal structure suggests that the method of network design by analogy to prototypic structures should be very effective.

The crystal structure of $[Ag(TEB)CF_3SO_3]$ (**4**) is homeotypic with the LaPtSi structure. In contrast to the LaPtSi structure where each of the atoms are roughly comparable in size, the tritopic ligand **2** is significantly larger than either the Ag(I) or the $CF_3SO_3^-$ ions. As a result, a single LaPtSi type net constructed with the dimensions of the tritopic ligand **2** and Ag(I) generates large void spaces. The triflate anion is of insufficient size to occupy fully these voids. The voids along [010] and [001] are filled by the six mutually independent, interpenetrating LaPtSi type lattices that constitute the $[Ag(TEB)\text{-}CF_3SO_3]\cdot(C_6H_6)_2$ structure (Fig. 2*C*)[24–27]. We note that the interpenetration occurs in such a way as to accommodate the propensity of aromatic rings to lie in a slightly staggered coplanar arrangement with an offset angle (α) 37° at an interplanar distance (d) of ~3.3 Å (Fig. 2*B*). To accommodate the geometrical requirements[28] (α and d) for stacking of the aromatic rings, the

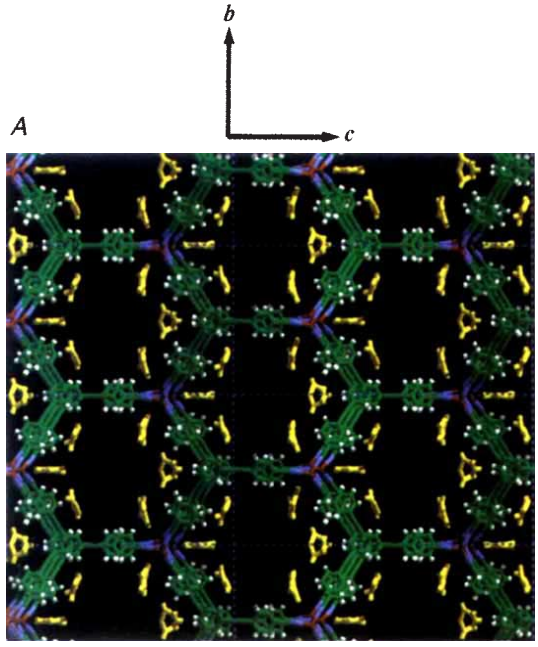

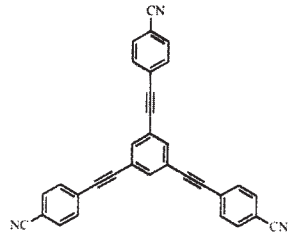

TEB (2)

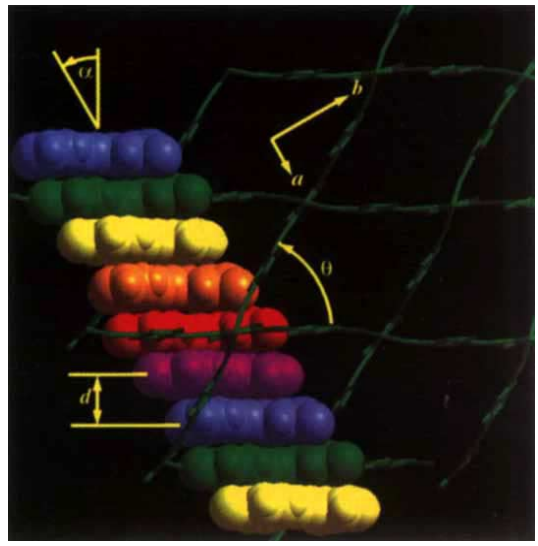

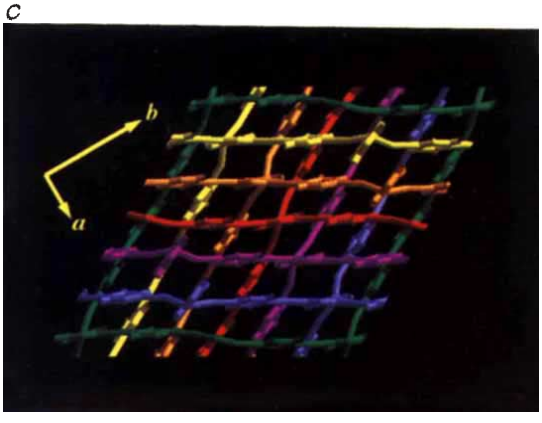

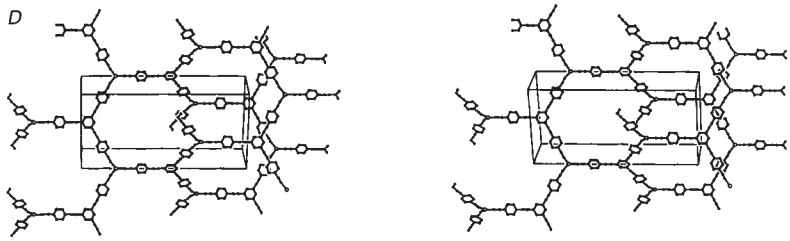

FIG. 2. *A*, Illustration of the 15-Å channels along [100] (*a* axis) in the crystal structure of **4**. The space within the channel is filled with benzene (shown yellow) which could readily be exchanged with C_6D_6. The carbon atoms are shown as green, hydrogen as white, nitrogen as blue and silver as brown. The triflate counterions have been removed for clarity. The chemical structure of a molecule of TEB (**2**) is also shown. *B*, Illustration of the stacking of the aromatic rings in the interpenetrated nets. Stacking occurs at a distance (d) of 3.3 Å with an offset angle α of ~37°. The shear angle (θ) of the net is 60°. This arrangement simultaneously accommodates the geometric requirements (α amd d) for the six independent self-included nets. *C*, Six independent nets interpenetrate to fill space along [010] (*b*-axis). *D*, Stereoview of a single LaPtSi type net of the crystal structure of **4**, showing the molecular constituents of the framework.

nets are sheared to an angle (θ) of 60° ($\theta = 90°$ for an ideal LaPtSi net, and 0° for CaCuP). However, the interpenetration leaves the channels along [100] near the maximum size possible for this network, as seen in Fig. 2*A*. This cavity of diameter 15 Å is filled by the solvent molecules. The coordinates of 12 benzene molecules per unit cell were located in the refinement.

Although such channels suggest a porous structure, they do not by themselves prove that the channels support reversible exchange of guest species. To demonstrate porosity, samples of $[Ag(TEB)CF_3SO_3]\cdot(C_6H_6)_2$ crystals were grown from benzene. The crystals were sieved through a 120-mesh screen to remove all small crystallites. Powder X-ray diffraction studies of these crystals showed that the product was quantitatively pure, and was the same phase as the single-crystal structure. Powder-diffraction data also showed that these crystals lose their crystallinity on loss of solvent. The large crystals were then placed in C_6D_6 (isotopic purity >99.5%) at room temperature, and subsequently washed with fresh C_6D_6 solution five times over the course of 3.5 days. The crystals were then placed in C_6D_6 (isotopic purity >99.96%), and were washed with fresh C_6D_6 solution three times over a period of one hour. Identical samples were placed under an optical microscope, and the morphology of the crystals subjected to similar treatment were monitored as a function of time. Visual inspection showed that the sample changed very little in its overall crystalline morphology during this time period. In particular, there were no microscopically observable cracks, and the dimensions and shape of the crystal remained constant. The X-ray powder pattern of these crystals after washing with C_6D_6 (isotopic purity >99.96%) showed that they remained identical to the original structure. After dissolving these crystals in fully deuterated acetone, NMR spectroscopy showed (to the limits of detection) no peak at δ7.34, thereby indicating the absence of the original benzene. Thus, although the crystal appears to be structurally unchanged, the actual composition of the crystal has changed from $[Ag(TEB)CF_3SO_3]\cdot(C_6H_6)_2$ to $[Ag(TEB)CF_3SO_3]\cdot(C_6D_6)_2$ without dissolution and reformation of the lattice. This demonstrates that the $[Ag(TEB)CF_3SO_3]\cdot(C_6H_6)_2$ crystals are indeed porous to benzene exchange.

The examples described here provide further evidence for the efficacy of the rational design of crystalline solids by analogies with solid-state structural chemistry. We have shown that it is possible to prepare molecular-based LaPtSi and CaCuP analogues by appropriate design. These networks resemble the nets studied theoretically by Baughman and Galvão[4]. Although we cannot as yet exactly predict which of the possible structure types will form from any given set of molecular constituents, the number of potential structures can be reduced greatly. Experiments are underway to measure the auxetic properties of compound **4** and to probe the diffusion of various organic solvents into the crystals of this compound. □

Received 23 December 1994; accepted 3 April 1995.

1. Desiraju, G. R. *Crystal Engineering: the Design of Organic Solids* (Elsevier, New York, 1989).
2. MacDonald, J. W. & Whitesides, G. M. *Chem. Rev.* **94,** 2383–2420 (1994).
3. Lehn, J. M. *Pure appl. Chem.* **66,** 1961–1966 (1994).
4. Baughman, R. H. & Galvão, D. S. *Nature* **365,** 735–737 (1993).
5. Evans, K. E. & Hutchinson, I. J. *Nature* **353,** 124 (1991).
6. Lakes, R. *Adv. Mater.* **5,** 293–296 (1993).
7. Moore, J. S. & Lee, S. *Chem. Ind.* 556–560 (1994).
8. Zaworotko, M. J. *Chem. Soc. Rev.* **23,** 283–288 (1994).
9. Robson, R. *et al. Supramolecular Architecture* (ed. Bein, T.) Ch. 19 (ACS Symp. Ser. 499, American Chemical Soc., Washington DC., 1992).
10. Lima-de-Faria, J., Hellner, E., Liebau, F., Makovicky, E. & Parthé, E. *Acta Crystallogr.* A**46,** 1–11 (1990).
11. Diederich, F. & Rubin, R. *Angew. Chem. int. Edn engl.* **31,** 1101–1123 (1992).
12. Hoffmann, R., Hughbanks, T., Kertész, M. & Bird, P. H. *J. Am. chem. Soc.* **105,** 4831–4832 (1983).
13. Zheng, C. & Hoffmann, R. *Inorg. Chem.* **28,** 1074–1080 (1989).
14. Wu, Z., Lee, S. & Moore, J. S. *J. Am. chem. Soc.* **114,** 8730–8732 (1992).
15. Hoskins, B. F., Robson, R. & Scarlett, N. V. Y. *J. chem. Soc., chem. Commun.* 2025–2026 (1994).
16. Abrahams, B. F., Hoskins, B. F., Michail, D. M. & Robson, R. *Nature* **369,** 727–729 (1994).
17. Kaszynski, P., Friedli, A. C. & Michl, J. *J. Am. chem. Soc.* **114,** 601–620 (1992).
18. Simard, M., Su, D. & Wuest, J. D. *J. Am. chem. Soc.* **113,** 4696–4698 (1991).
19. Fagan, P. J., Ward, M. D. & Calabrese, J. C. *J. Am. chem. Soc.* **111,** 1698–1719 (1989).
20. Klepp, K. & Parthé, E. *Acta Crystallogr.* B**38,** 1105–1108 (1982).
21. Mewis, A. *Z. Naturforsch.* **33B,** 983–986 (1976).
22. Bailey, A. S., Henn, B. R. & Langdon, J. M. *Tetrahedron* **19,** 161–167 (1963).
23. Zhang, J., Pesak, D. J., Ludwick, J. L. & Moore, J. S. *J. Am. chem. Soc.* **116,** 4227–4239 (1994).
24. Wang, X., Simard, M. & Wuest, J. D. *J. Am. chem. Soc.* **116,** 12119–12120 (1994).
25. Duchamp, D. J. & Marsh, R. E. *Acta Crystallogr.* B**25,** 5–19 (1969).
26. Ermer, O. & Lindenberg, L. *Helv. chim. Acta.* **74,** 825–877 (1991).
27. Ermer, O. *J. Am. chem. Soc.* **110,** 3747–3754 (1988).
28. Gavezzotti, A. & Desiraju, G. R. *Acta Crystallogr.* B**44,** 427–434 (1988).
29. Sheldrick, G. M. *Crystal Solution Program* (Inst. für Anorg. Chemie, Gottingen, 1993).

SUPPLEMENTARY INFORMATION. Requests should be addressed to Mary Sheehan at the London editorial office of *Nature*.

ACKNOWLEDGEMENTS. We thank Siemens Inc. and in particular C. F. Camapana for collecting the data on **4**, and J. W. Kampf for collecting the data set on $[Ag(TCB)_3(CF_3SO_3)]$. J.S.M. thanks the US NSF, the NSF Young Investigator programme (1992–97), the Camille Dreyfus Teacher–Scholar Awards programme and the 3M company (non-tenured faculty awards programme) for their support. S.L. thanks the A. P. Sloan Foundation (1993–95) and the J. D. and C. T. MacArthur Foundation (1993–97) for fellowships.

Segmentation of mid-ocean ridges with an axial valley induced by small-scale mantle convection

Stéphane Rouzo, Michel Rabinowicz & Anne Briais

Groupe de Recherche de Géodésie Spatiale, CNRS UPR234 & UMR39, 14, Ave Edouard Belin, 31400 Toulouse, France

THE small-scale segmentation of mid-ocean ridges with an axial rise has been modelled by considering each ridge segment as a giant crack in the lithosphere with a tip propagating along the ridge axis[1,2]. For ridges with an axial valley, however, this type of model fails because the lithosphere is too thick to tear[3]. Yet such ridges are clearly segmented, as defined by morphology, gravity and structure at the 50–100 km length scale. The ridge offsets are large[4,5], and vary dramatically with time. This type of segmentation is commonly related to a three-dimensional, small-scale mantle flow occurring in the partially molten asthenosphere below the ridge[6–8]. Here we propose a model for segmentation in such ridges, in which the convective flow below the ridge favours an asymmetrical breaking of the axial-valley lithosphere. This leads to the development and separation of ridge segments in a pattern that mimics the observed geometry and temporal evolution of the segmentation of most ridges with an axial valley. If our model is correct, it implies that coupling of oceanic lithosphere to small-scale convection controls the dynamics of mid-ocean ridges.

Our model starts from the buoyant convective flow pictured in Fig. 1. In this case, convection generates rolls without any preferred orientation. At a mid-ocean ridge, however, the diverging plates induce shear at the surface. When included in the calculation, this shear forces the convective flow to orient the rolls parallel to the spreading direction (Fig. 2*a*). Because the flow adjusts to the boundary conditions extremely slowly, it retains the memory of the initial thermal conditions for a long time. Despite the symmetric shear, currents ascending below the ridge remain asymmetric about the spreading axis, even after 150 Myr of evolution. The continuing asymmetry in the convective pattern in turn produces an asymmetric stress field in the lithosphere. We now show how these asymmetrical stresses are able to split a straight ridge axis into segments whose lengths and offsets continue to vary for several hundred million years.

Ridges with an axial valley exhibit an average axial lithospheric thickness of 8 km (refs 9–11). The valley results from the necking of this thick lithosphere[12,13], stretched by large-scale horizontal stresses (20–30 MPa)[14], and accreted from below by